

Article

Soil Moisture Mapping Using Multi-Frequency and Multi-Coil Electromagnetic Induction Sensors on Managed Podzols

Emmanuel Badewa ¹, Adrian Unc ¹ , Mumtaz Cheema ¹, Vanessa Kavanagh ² and Lakshman Galagedara ^{1,*} 

¹ School of Science and the Environment, Grenfell Campus, Memorial University of Newfoundland, Corner Brook, NL A2H 5G4, Canada; eab577@grenfell.mun.ca (E.B.); aunc@grenfell.mun.ca (A.U.); mcheema@grenfell.mun.ca (M.C.)

² Department of Fisheries and Land Resources, Government of Newfoundland and Labrador, Pasadena, NL A0L 1K0, Canada; VanessaKavanagh@gov.nl.ca

* Correspondence: lgalagedara@grenfell.mun.ca; Tel.: +1-(709)-639-2565

Received: 15 August 2018; Accepted: 8 October 2018; Published: 10 October 2018



Abstract: Precision agriculture (PA) involves the management of agricultural fields including spatial information of soil properties derived from apparent electrical conductivity (EC_a) measurements. While this approach is gaining much attention in agricultural management, farmed podzolic soils are under-represented in the relevant literature. This study: (i) established the relationship between EC_a and soil moisture content (SMC) measured using time domain reflectometry (TDR); and (ii) evaluated the estimated SMC with EC_a measurements obtained with two electromagnetic induction (EMI) sensors, i.e., multi-coil and multi-frequency, using TDR measured SMC. Measurements were taken on several plots at Pynn's Brook Research Station, Pasadena, Newfoundland, Canada. The means of EC_a measurements were calculated for the same sampling location in each plot. The linear regression models generated for SMC using the CMD-MINIEXPLORER were statistically significant with the highest R^2 of 0.79 and the lowest RMSE (root mean square error) of $0.015 \text{ m}^3 \text{ m}^{-3}$ but were not significant for GEM-2 with the lowest R^2 of 0.17 and RMSE of $0.045 \text{ m}^3 \text{ m}^{-3}$; this was due to the difference in the depth of investigation between the two EMI sensors. The validation of the SMC regression models for the two EMI sensors produced the highest $R^2 = 0.54$ with the lowest RMSE prediction = $0.031 \text{ m}^3 \text{ m}^{-3}$ given by CMD-MINIEXPLORER. The result demonstrated that the CMD-MINIEXPLORER based measurements better predicted shallow SMC, while deeper SMC was better predicted by GEM-2 measurements. In addition, the EC_a measurements obtained through either multi-coil or multi-frequency sensors have the potential to be successfully employed for SMC mapping at the field scale.

Keywords: apparent electrical conductivity; precision agriculture; soil moisture content; electromagnetic induction

1. Introduction

Development of site-specific management (SSM) over large fields is the goal of precision agriculture (PA). PA encompasses the use of spatial and temporal information to support decisions on agronomic practices that best match soil and crop requirements as they vary in the field [1,2]. Lesch et al. [3] have shown that different types of spatial information such as soil texture and salinity derived from bulk apparent electrical conductivity (EC_a) obtained by electromagnetic induction (EMI) surveys can offer significant support to the development of accurate management decisions for agricultural fields. PA provides a way to automate SSM using information technology, thereby making

SSM practical in commercial agriculture. It includes all those agricultural production practices that use information technology either to tailor input to achieve desired outcomes, or to monitor those outcomes (e.g., variable rate application of pesticides and fertilizers) [4]. Hence, the measurement of EC_a using the EMI technology has been proposed as an effective and rapid response methodology in support of PA [5,6].

Literature shows that EC_a has the potential to become a widely adopted means for characterizing the spatial variability of soil properties at field and landscape scales [7,8]. Spatial variability of soil properties can also be characterized by other means such as ground penetrating radar (GPR) [9,10], time domain reflectometry (TDR) [11,12], cosmic-ray neutrons [13,14], aerial photography [5,15], multi- and hyper-spectral imagery [16,17], or by a combination of several approaches as shown by Rudolph et al. [18].

Soil Moisture Content (SMC) is a major factor that influences EC_a and agricultural practices. Factors affecting EC_a include SMC , soil temperature, high clay content, and soluble salts (i.e., pore water conductivity) [19–22]. When soil salinity, texture, mineralogy and temperature are constant, EC_a is a direct function of SMC [23,24]. Under such conditions, several authors have established that there is a linear relationship between SMC and EC_a [25–28]. However, other researchers have established relationships between EC_a and other soil properties such as soil salinity [29,30], saturated percentage [7,31] and soil bulk density [32,33]. Furthermore, SMC is widely recognized as a driving factor for agricultural productivity as it governs germination and plant growth [34]. Given the time, labour, and cost of traditional soil sampling (Huang et al. 2014) [35], the development of an accurate proxy alternative for measuring the spatio-temporal variability of SMC , such as EMI, is essential for efficient soil and crop management at large scales [36].

Few research studies have been conducted to evaluate the potential of multi-coil and multi-frequency EMI sensors such as CMD-MINIEXPLORER (GF Instruments, Brno, Czech Republic) and GEM-2 (Geophex Ltd., Raleigh, NC, USA), respectively, to estimate soil properties. Multi-coil EMI sensors have multiple coil spacing and coil orientations which operate with one frequency and have one transmitter and three coplanar receiver coils at different distances [33]. Multi-frequency EMI sensors have different frequencies and coil orientations which operate with one transmitter coil and a receiver coil separated at a specific distance [37]. In general, the theoretical depth of investigations (DOIs) is calculated based on the knowledge of coil separation and frequency [38,39]. Most research studies to date have adopted the use of EMI instruments to estimate soil properties under different soils and crop systems e.g., [40–42]; however, the use of multi-coil and multi-frequency EMI sensors to determine the variability in podzolic soils is still limited [43]. This might be attributed to the noisy data and low EC_a values generated from the application of EMI sensors to podzolic soils.

Podzols are coarse to medium textured soils formed from acidic parent material. They are distinctively characterized by illuviated B horizons where humified organic matter combined in varying degrees with Al and Fe accumulate, often overlain by a light coloured eluviated (Ae) horizon [44]. Globally, podzolic soils are widely spread in the temperate and boreal regions of the Northern Hemisphere and occupy approximately 4% (485 million ha) of the earth's total land surface [45]. The adaptation of podzolic soils for agriculture is growing because of the increased demand on the current agricultural land base, application of intensive mechanization, fertilization, and water management practices [46], and is favoured by climate-change related northward shift in favourable climatic parameters [47]. In addition, due to podzolic soils' distinctive morphology, the conversion to agricultural land can significantly affect their hydrological parameters such as SMC [48,49]. Despite their uniqueness, there is limited information available on water management on podzolic soils for effective agricultural production [46]. Furthermore, literature suggests that little or no work has been carried out to estimate spatio-temporal variability of SMC for managed podzols [43].

The objectives of this study were: (i) to evaluate the multi-coil (CMD-MINIEXPLORER) and multi-frequency (GEM-2) EMI sensor data and the various combinations of these instruments for agricultural systems on managed podzols; (ii) to develop a relationship between EC_a , as estimated by

both instruments, and SMC measured using HD2-TDR; and (iii) to estimate the accuracy of regression models between the EC_a and SMC .

2. Materials and Method

2.1. Study Site

The study was carried out at Pynn's Brook Research Station (PBRS) ($49^{\circ}04'20''$ N, $57^{\circ}33'35''$ W), Pasadena, Newfoundland (Figure 1), Canada. The reddish brown to brown podzolic soil developed on a gravelly sandy fluvial deposit with > 100 cm depth to bedrock and a 2%–5% slope [50]. Soil samples from the topsoil ($n = 7$) analysed for the study site revealed a gravelly loamy sand soil (sand = 82.0% (± 3.4); silt = 11.6% (± 2.4); clay = 6.4% (± 1.2)), which is classified as orthic Humo-ferric podzol, according to Canadian Soil Taxonomy [50]. The average bulk density and porosity for the study site ($n = 28$) at 15 cm soil depth were 1.31 g cm^{-3} (± 0.07) and 51% (± 0.03), respectively. Based on the 30-year data (1986–2016) of the nearby Deer Lake weather station from Environment Canada (<http://climate.weather.gc.ca/>), the area receives an average precipitation of 1113 mm per year with less than 410 mm falling as snow, and has an annual mean temperature of 4°C .

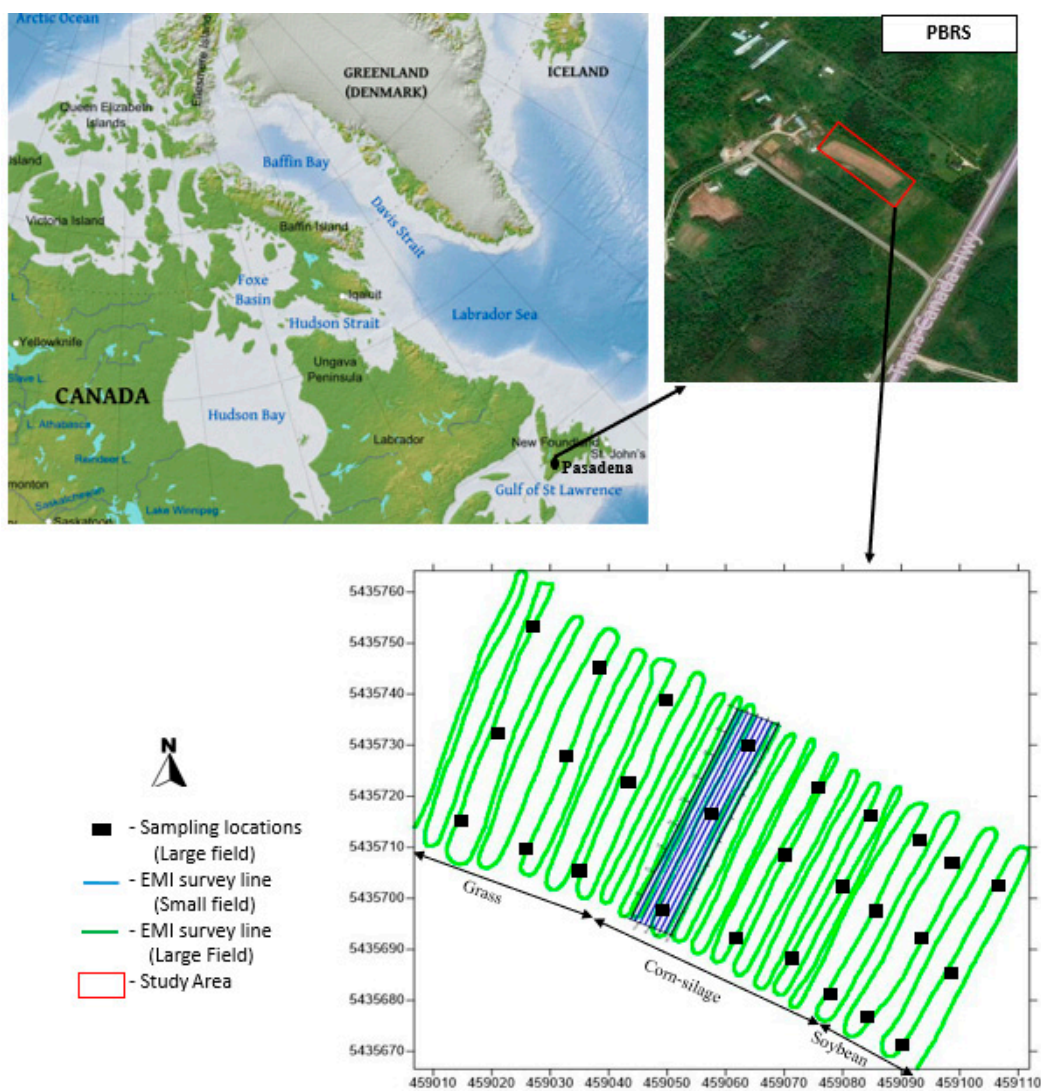


Figure 1. The location of Pynn's Brook Research Station (PBRS), Pasadena ($49^{\circ}04'20''$ N, $57^{\circ}33'35''$ W) in Newfoundland, Canada and the study site.

2.2. SMC Data Recording and TDR Calibration

During the study, SMC was measured using a hand-held time domain reflectometry (TDR) probe. The TDR measured SMC data were first compared with the calculated SMC, which was determined by multiplying gravimetric SMC (θ_g) with the measured average soil bulk density of 1.31 g cm^{-3} . The TDR measured SMC was compared with the calculated SMC to evaluate the field scale accuracy of the TDR probe. The average gravimetric SMC, θ_g (g g^{-1}) was determined for the 0–20 cm ($\theta_{g(0-20)}$) depth range by oven drying moist soil samples at 105°C for 48 h. An integrated TDR, known as HD2-TDR (IMKO Micromodultechnik GmbH, Germany) with probe lengths of 11 cm ($\theta_{v(0-11)}$), 16 cm ($\theta_{v(0-16)}$) and 30 cm ($\theta_{v(0-30)}$) [51] was used. Also, the mean soil temperature measured from the HD2-TDR precision soil moisture probe was used for the temperature conversion of measured EC_a data.

2.3. EMI Survey

In this study, EC_a was measured using the multi-coil CMD-MINIEXPLORER (GF instruments, Brno, Czech Republic) and the multi-frequency GEM-2 (Geophex, Ltd., Raleigh, NC, USA). The CMD-MINIEXPLORER has 3 coil separations and can be operated at vertical coplanar (VCP) and horizontal coplanar (HCP) coil configurations. The CMD-MINIEXPLORER therefore generates six pseudo depths (PDs), also known as depths of investigation (DOI), of 25, 50 and 90 cm when using VCP modes, and 50, 100, 180 cm when using HCP modes [33]. The theoretical calculation of the DOI for GEM-2 is at a deeper depth compared to the CMD-MINIEXPLORER [52]. However, the accuracy of the DOI of GEM-2 with varying frequencies under heterogenic field conditions is yet to be determined. Based on the preliminary data obtained on the site, the CMD-MINIEXPLORER with the largest coil separation (coil 3 = 118 cm) with PDs of 90 and 180 for VCP and HCP modes, respectively, and a 38 kHz frequency of GEM-2 (the coil separation is 166 cm) were employed in this study. The CMD-MINIEXPLORER at the VCP configuration is represented with EC_a -L and at the HCP configuration is represented with EC_a -H while GEM-2 at the HCP configuration is represented with EC_a -38 kHz. Surveys with CMD-MINIEXPLORER were conducted at a height of 15 cm. The GEM-2 device was carried with the supplied shoulder strap at an average height of 100 cm.

Several studies suggested temperature conversion of raw EC_a to a standard soil temperature (25°C) e.g., [1,53] using:

$$EC_{25} = EC_t \times (0.4470 + 1.4034 e^{-t/26.815}) \quad (1)$$

where EC_t is the EC_a data collected at measured soil temperature ($^\circ\text{C}$) and EC_{25} is the temperature corrected EC_a .

To avoid data shifts, both sensors were allowed a warm up period of at least 30 min before measurements were recorded [54]. However, no instrumental drift was expected in the EC_a due to the high temperature stability of the CMD-MINIEXPLORER and GEM-2 [37,55].

EMI surveys were conducted on a small field ($45 \text{ m} \times 8.5 \text{ m}$) and a large field (0.45 ha) using CMD-MINIEXPLORER and GEM-2. The large field comprises of the grass, silage-corn and soybean plots while the small field is a portion of the silage-corn experimental plot selected for a detailed field study (Figure 1). The EC_a measurements were carried out on 30 September, 6 October, and 18 November in Fall 2016, and on 31 May in Spring 2017. The relationship between CMD-MINIEXPLORER and GEM-2 was assessed by comparing the patterns and trends of measured EC_a data from both instruments using a 45 m linear transect collected on 30 September on the small field.

2.4. Field Calibration and Validation

The small field was used to calibrate and validate the relationship between SMC and EC_a using data collected on 30 September and 6 October 2016, respectively. The calibration was carried out using the EC_a data (EC_a -L, EC_a -H and EC_a -38 kHz) and measured SMC data collected with the HD2-TDR probes (0–11, 0–16, and 0–30 cm) on 30 September 2016. The validation was then carried out using the EC_a data and HD2-TDR measured SMC at 0–11 and 0–16 cm depths on 6 October 2016. The validation

was further carried out on a 30 m transect on the silage-corn plot and the grass plot at the study site using the data collected on 31 May 2017. The small field survey was carried out on a gridded plot (without GPS) for constant precise point calibration and validation. The proximally sensed EC_a was determined using the mean EC_a measurements ($n = 20$) generated on the small field from CMD-MINIEXPLORER and GEM-2 survey data collected on the same day along each of the selected twenty sampling locations similar to Zhu et al. [56].

To test EC_a response to SMC variability at a larger spatial scale, a large field study was conducted to validate the regression model generated from the small field on 18 November 2016. The EMI survey on the large field was carried out by walking across the entire field with a GPS connected to CMD-MINIEXPLORER and GEM-2 to obtain geo-referenced EC_a data. Also, twenty-seven geo-referenced SMC data points ($\theta_{v(0-16)}$) were collected using the HD2-TDR 0–16 cm length probe only and a hand held GPS according to the stratified sampling locations.

2.5. Soil Sampling

The silage-corn trial on the small field consisted of 4 m × 1 m plots that received different nutrient management treatments using biochar (BC), dairy manure (DM), inorganic fertilizer, or a combination of these. Soil samplings on the small field were done by selecting twenty sampling locations based on the BC and DM application, though the treatment effects were not significant across the small field [28]. Soil samples were collected from the depths of 0–10 cm and 10–20 cm using a gouge auger and a hammer. Samples were placed in airtight bags and stored in a polystyrene cooler until gravimetric SMC (θ_g) measurements were carried out in the laboratory.

2.6. Data Analysis

Descriptive statistics (min, max, mean, median, skewness, kurtosis and coefficient of variation, CV) were carried out to evaluate the EMI data and SMC data. Paired sample *t*-tests were carried out to determine if there were any statistically significant differences between the EC_a and SMC means. Pearson's correlation coefficients (*r*) were used to establish the relationship between EC_a data and SMC data. The coefficient of determination (R^2) was used to evaluate the relationship among EMI results. The root mean square error (RMSE) was used to evaluate the accuracy of the HD2-TDR measured SMC. The root mean square error of prediction (RMSEP) was used to estimate the accuracy of predicted SMC using the EC_a and TDR measured SMC data. A simple linear regression was used to evaluate the relationship between EC_a and SMC data. All analyses were performed with Minitab 17 (Minitab 17 Statistical Software, 2010) and EC_a maps were generated using Surfer 8 (Golden Software, 2002).

3. Results

3.1. SMC Results

A good match between the measured SMC (θ_v) from HD2-TDR and the calculated SMC (θ_v) by using gravimetric SMC (θ_g) was obtained, with an R^2 of >0.88 and a $RMSE < 0.04 \text{ m}^3 \text{ m}^{-3}$ for all three TDR probe lengths (Figure 2 and Table 1). Accuracy of the HD2-TDR for the 16 cm probe length is similar to the $RMSE$ of $0.013 \text{ m}^3 \text{ m}^{-3}$ by Topp et al. [11] while the HD2-TDR for the 11 and 30 cm probe lengths has $RMSE$ values of $0.040 \text{ m}^3 \text{ m}^{-3}$ and $0.018 \text{ m}^3 \text{ m}^{-3}$, respectively (Figure 2 and Table 1).

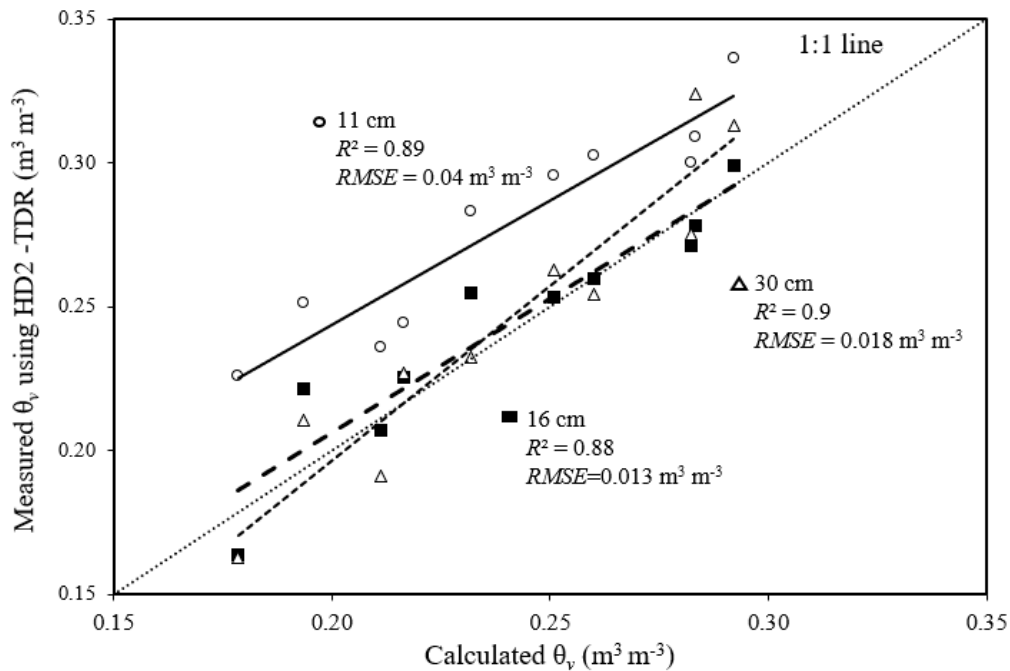


Figure 2. Comparison of the measured θ_v using the HD2-TDR and calculated θ_v by using the measured θ_g and bulk density at Pynn’s Brook Research Station.

Table 1. Linear regression, coefficient of determination (R^2) and root mean square error (RMSE) for HD2-TDR calibration at Pynn’s Brook Research Station using the calculated θ_v from θ_g ($n = 10$).

SMC	Regression Equation	R^2	RMSE
$\theta_{v(0-11)}$	$0.8646 (\theta_v) + 0.0708$	0.89	0.040
$\theta_{v(0-16)}$	$0.9330 (\theta_v) + 0.0193$	0.88	0.013
$\theta_{v(0-30)}$	$1.2137 (\theta_v) - 0.0462$	0.90	0.018

3.2. EMI Results

The EC_a patterns and trends along the 45 m transect on the small field were similar for CMD-MINIEXPLORER and GEM-2, despite different DOIs (Figures 3 and 4). The data from CMD-MINIEXPLORER plotted against the GEM-2 data (Figure 5) show that EC_a values of EC_a -H are closely associated to that of GEM-2 ($R^2 = 0.71$) compared to EC_a -L ($R^2 = 0.40$). The possibility of integrating the mean EC_a measurements from the CMD-MINIEXPLORER and the GEM-2 was evaluated with the average of EC_a -L, EC_a -H and EC_a -38 kHz and analysed using the backward stepwise multiple linear regression (MLR). The results indicated that they were redundant.

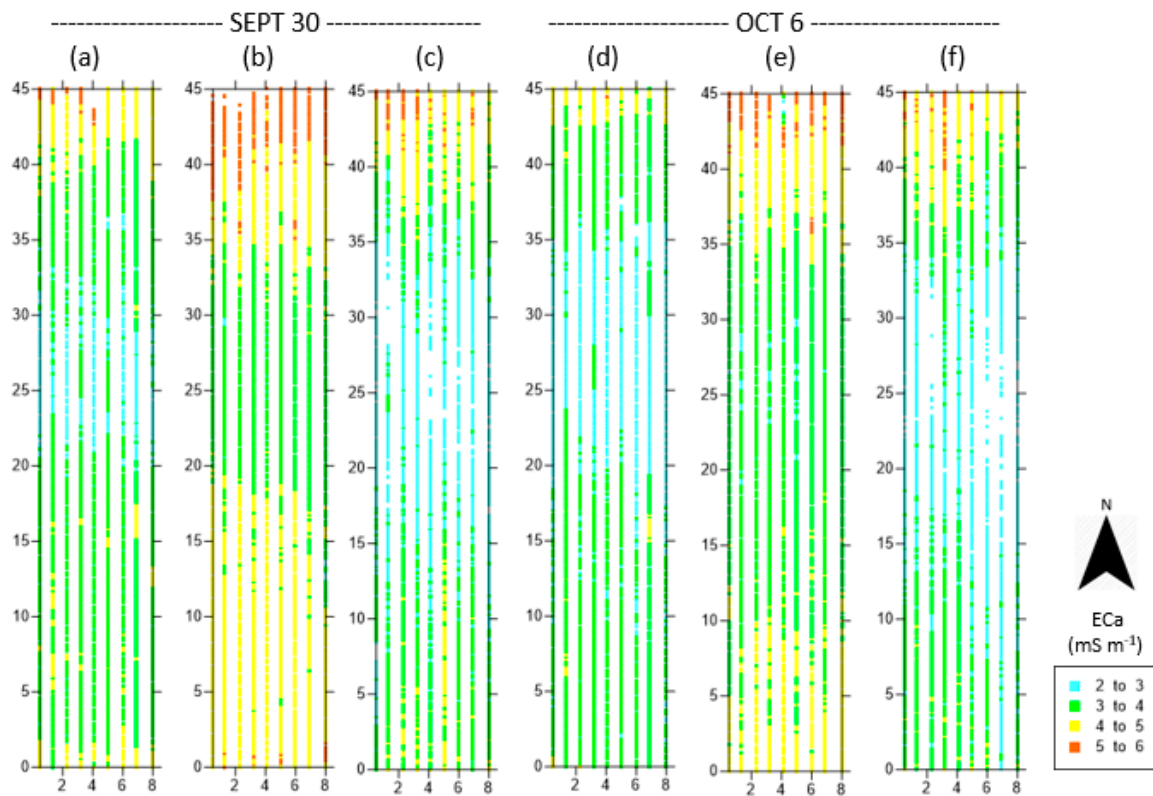


Figure 3. Results of small field EMI surveys on 30 September and 6 October 2016 for EC_a -L (a,d), EC_a -H (b,e) and EC_a -38 kHz (c,f).

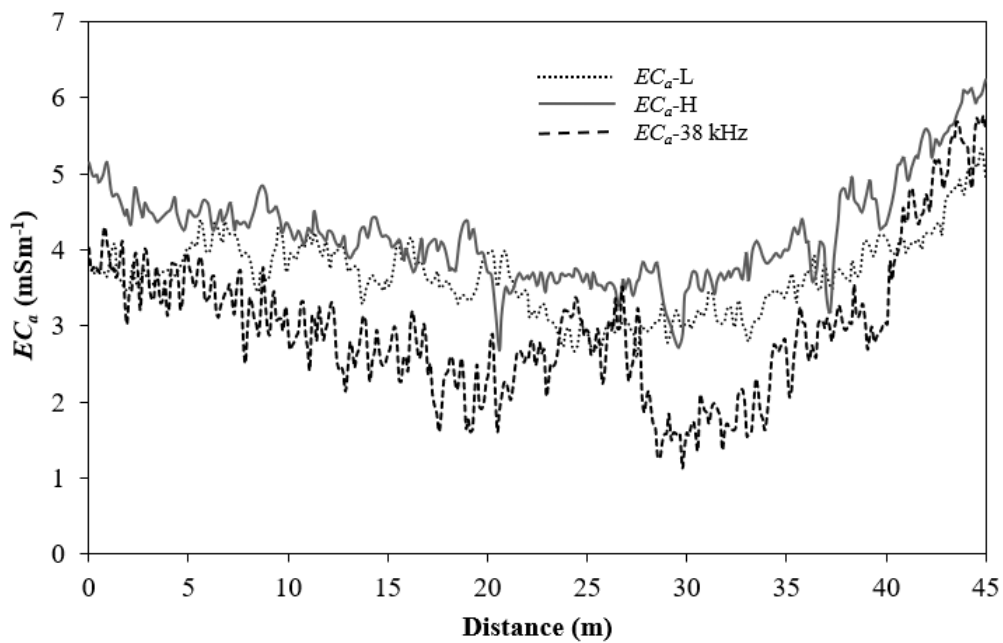


Figure 4. Variability of the measured EC_a by the two EMI sensors on a 45 m linear transect in the small field.

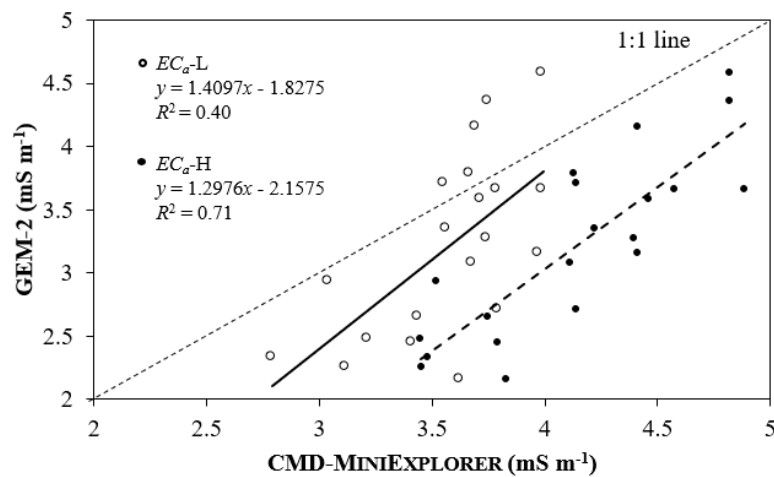


Figure 5. Scatter-plot of EC_a measured using CMD-MINIEXPLORER and GEM-2.

3.3. Basic Statistics

The descriptive statistics of the EC_a measurements from CMD-MINIEXPLORER, GEM-2 and the TDR measured SMC in the study site are given in Table 2. According to the classification of Warrick and Nielsen [57], CVs of CMD-MINIEXPLORER were low ($CV < 12\%$) while those of GEM-2 were moderate ($12\% < CV < 62\%$). The CVs of TDR measured SMC were moderate ($CV > 12\%$) except for the $\theta_{v(0-11)}$ depth, which was low (Table 2).

Table 2. Descriptive statistics of the EC_a ($mS\ m^{-1}$) measurements using CMD-MINIEXPLORER and GEM-2 and TDR measured SMC ($m^3\ m^{-3}$) at the study site ($n = 20$).

Depth	Min	Max	Mean	Median	Skewness	Kurtosis	CV
EC_a -L	2.79	3.99	3.58 a	3.68	-0.9	0.5	9.0
EC_a -H	3.45	4.88	4.14 a	4.14	-0.1	-1.0	11.3
EC_a -38 kHz	2.15	4.58	3.21 b	3.2	0.2	-0.9	22.4
$\theta_{v(0-11)}$	0.23	0.34	0.29 c	0.30	-0.5	-0.6	11.3
$\theta_{v(0-16)}$	0.16	0.31	0.25 d	0.26	-0.7	0.2	14.6
$\theta_{v(0-30)}$	0.16	0.35	0.25 d	0.26	0.1	-0.4	20.5

Means that do not share a letter are significantly different at 5% probability.

A paired sample t -test was performed using a sample of 20 EC_a data points from the small field to determine whether there was a difference between means of EC_a from CMD-MINIEXPLORER and GEM-2. Results revealed that EC_a means of EC_a -38 kHz (3.214 ± 0.718) were significantly different from EC_a -L (3.576 ± 0.323) and EC_a -H (4.139 ± 0.466), with $p = 0.050$ and $p = 0.000$, respectively.

A paired sample t -test was also carried out on a sample of 20 SMC data points to determine whether there was a difference in the SMC means at different depths. The SMC mean for $\theta_{v(0-11)}$ (0.28755 ± 0.03241) was significantly different from the means obtained for $\theta_{v(0-16)}$ (0.25268 ± 0.03690) and $\theta_{v(0-30)}$ (0.2471 ± 0.0507); both differences had the same $p = 0.000$. Pearson's correlation coefficients among EC_a measurements and SMC are shown in Table 3. At a p -value < 0.1 , EC_a data (CMD-MINIEXPLORER and GEM-2) were significantly correlated with SMC measurements.

Table 3. Pearson’s correlation coefficients of the EC_a measurements of CMD-MINIEXPLORER and GEM-2 and TDR measured SMC at the study site ($n = 20$). Significance is reported at the 0.1 (*), 0.05 (**), and 0.001 (***) p -values.

	EC_a -L	EC_a -H	EC_a -38 kHz	$\theta_{v(0-11)}$	$\theta_{v(0-16)}$	$\theta_{v(0-30)}$
EC_a -L	1					
EC_a -H	0.88 ***	1				
EC_a -38 kHz	0.63 **	0.84 ***	1			
$\theta_{v(0-11)}$	0.89 ***	0.74 ***	0.54 **	1		
$\theta_{v(0-16)}$	0.86 ***	0.68 ***	0.50 **	0.95 ***	1	
$\theta_{v(0-30)}$	0.59 **	0.42 *	0.41 *	0.75 ***	0.79 ***	1

3.4. Regression Analysis

The fitted linear regressions (LRs) to estimate SMC for different integral depths using measured EC_a with CMD-MINIEXPLORER or GEM-2 data are shown in Figure 6 and respective statistics for calibration and validation between EC_a and TDR measured SMC are summarized in Table 4. The SMC estimates obtained using EC_a -L ($R^2_p = 0.38$ and 0.54) are better than the estimates for EC_a -H and EC_a -38 kHz, with $RMSEP$ 0.033 and 0.031 $m^3 m^{-3}$, respectively (Table 4).

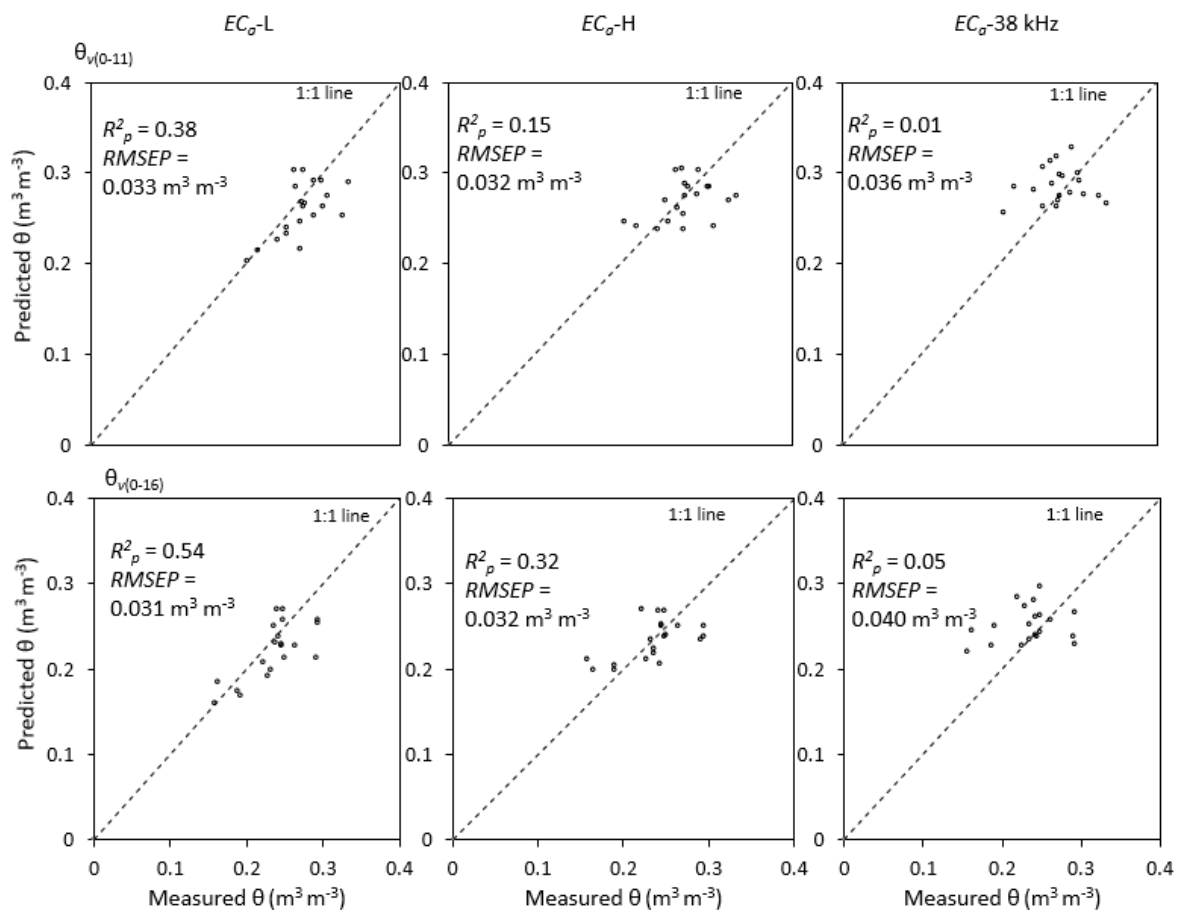


Figure 6. Plots of predicted θ_v ($m^3 m^{-3}$) using EC_a data versus TDR measured θ_v ($m^3 m^{-3}$) for the linear regressions given in Table 4 for EC_a -L, EC_a -H and EC_a -38 kHz.

Table 4. Linear regressions between EC_a data from CMD-MINIEXPLORER and GEM-2 with TDR measured SMC for different integral depths ($n = 20$).

EC_a	SMC	Regression Equation	Calibration		Validation	
			R^2	RMSE	R^2_p	RMSEP
EC_a -L	$\theta_{v(0-11)}$	$0.0888 EC_a$ -L $- 0.0301$	0.79	0.015	0.38	0.033
	$\theta_{v(0-16)}$	$0.0983 EC_a$ -L $- 0.0988$	0.74	0.018	0.54	0.031
	$\theta_{v(0-30)}$	$0.0925 EC_a$ -L $- 0.0836$	0.35	0.040	-	-
EC_a -H	$\theta_{v(0-11)}$	$0.0515 EC_a$ -H $+ 0.0743$	0.55	0.021	0.15	0.032
	$\theta_{v(0-16)}$	$0.0542 EC_a$ -H $+ 0.0284$	0.47	0.026	0.32	0.031
	$\theta_{v(0-30)}$	$0.0462 EC_a$ -H $+ 0.056$	0.18	0.045	-	-
EC_a -38 kHz	$\theta_{v(0-11)}$	$0.0243 EC_a$ -38 kHz $+ 0.2095$	0.29	0.027	0.01	0.036
	$\theta_{v(0-16)}$	$0.0257 EC_a$ -38 kHz $+ 0.1701$	0.25	0.031	0.05	0.040
	$\theta_{v(0-30)}$	$0.0292 EC_a$ -38 kHz $+ 0.1533$	0.17	0.045	-	-

Because the purpose of the large field study was to evaluate the EC_a response to variability in SMC at a larger spatial scale, only the $\theta_{v(0-16)}$ depth with the highest accuracy for the study site (Table 1) was measured at 27 geo-referenced locations on the field. The linear regression between $\theta_{v(0-16)}$ and EC_a -L on the small field was used for the large field study. The estimates of SMC for $\theta_{v(0-16)}$ using EC_a -L were lower for the large field study than for the small field study ($RMSEP = 0.076 \text{ m}^3 \text{ m}^{-3}$).

The same linear regressions were applied to a 30 m transect in the corn-silage plot and the grass plot at the study site (Table 5) for validation of linear regressions. The estimates of SMC via EC_a -L for the grass plot had lower R^2 values (from 0.07 to 0.32) and higher $RMSEP$ (from 0.039 to $0.074 \text{ m}^3 \text{ m}^{-3}$) than for the silage-corn plot ($R^2 =$ from 0.30 to 0.59; $RMSEP =$ from 0.041 to $0.072 \text{ m}^3 \text{ m}^{-3}$). Overall, fitted linear regressions developed between EC_a and SMC in this study have shown higher prediction accuracy for EC_a -L than for EC_a -H and EC_a -38 kHz.

Table 5. Validation of the fitted linear regressions summarised in Table 4, using EC_a data from CMD-MINIEXPLORER and GEM-2 with TDR measured SMC on a 30 m transect ($n = 11$).

SMC	EC_a	Silage Corn Plot		Grass Plot	
		R^2_p	RMSEP	R^2_p	RMSEP
$\theta_{v(0-11)}$	EC_a -L	0.30	0.046	0.13	0.066
	EC_a -H	0.35	0.054	0.32	0.062
	EC_a -38 kHz	0.30	0.041	0.30	0.074
$\theta_{v(0-16)}$	EC_a -L	0.55	0.070	0.07	0.071
	EC_a -H	0.58	0.044	0.26	0.053
	EC_a -38 kHz	0.59	0.072	0.23	0.061
$\theta_{v(0-30)}$	EC_a -L	-	-	0.07	0.062
	EC_a -H	-	-	0.18	0.039
	EC_a -38 kHz	-	-	0.14	0.040

3.5. EC_a Mapping

The spatial variability of EC_a was mapped across the study site by variogram analysis and ordinary block kriging using Surfer 8 (Golden Software, 2002, Golden, CO, USA). The trends of EC_a data from the CMD-MINIEXPLORER and the GEM-2 show similar patterns despite different DOIs (or sampling volume) and EC_a values (Figure 7). For instance, larger EC_a values were measured at the northwest and southeast sections of the study site while lower EC_a values were found on the northeast section, which stretches across the middle area of the field. The map of SMC predicted using the EC_a -L and the 27 georeferenced measurements (Figure 8) shows similar patterns with lower values ($<0.28 \text{ m}^3 \text{ m}^{-3}$) across the centre of the study site.

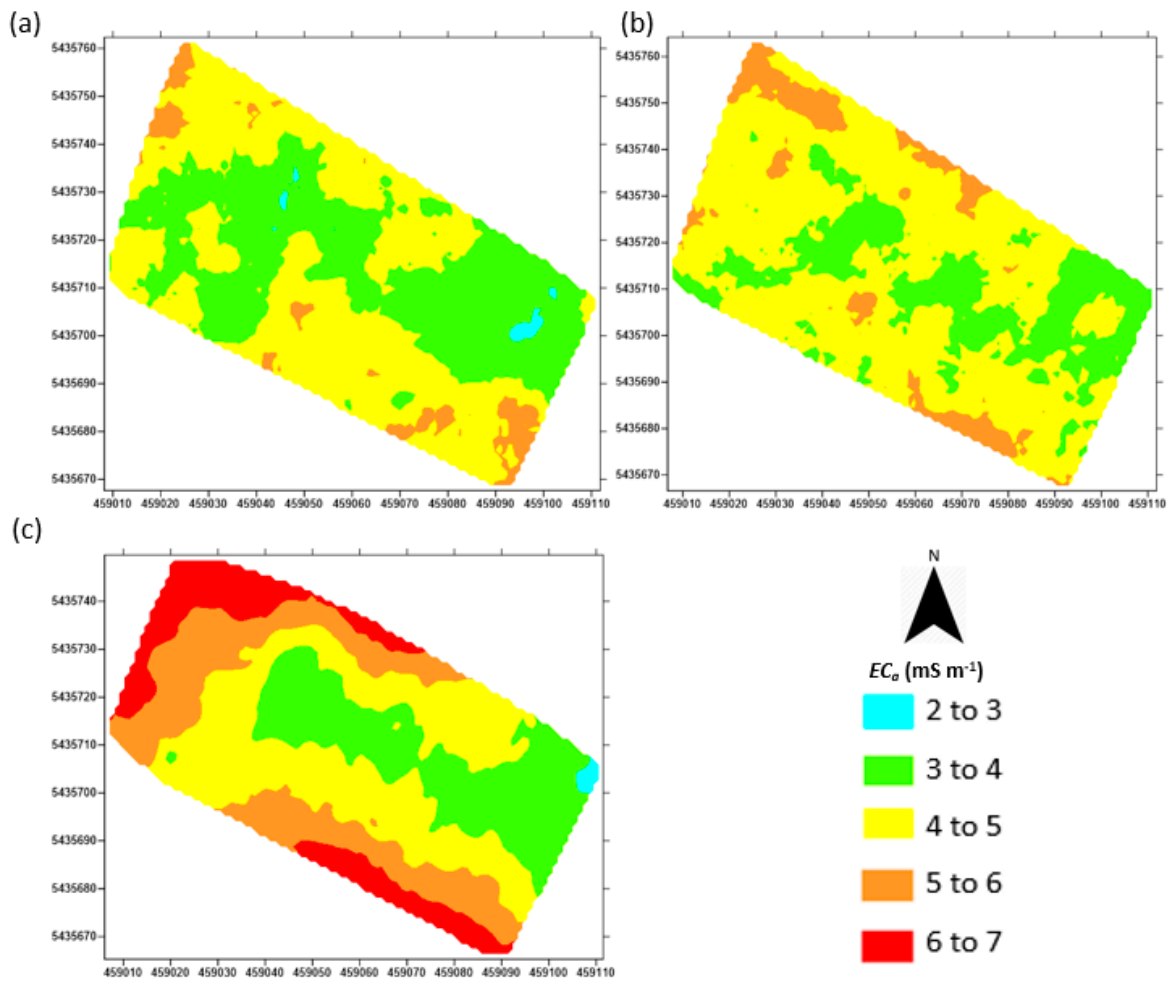


Figure 7. Spatial variability maps of EC_a for the large field study (a) EC_a -L (b) EC_a -H (c) EC_a -38 kHz.

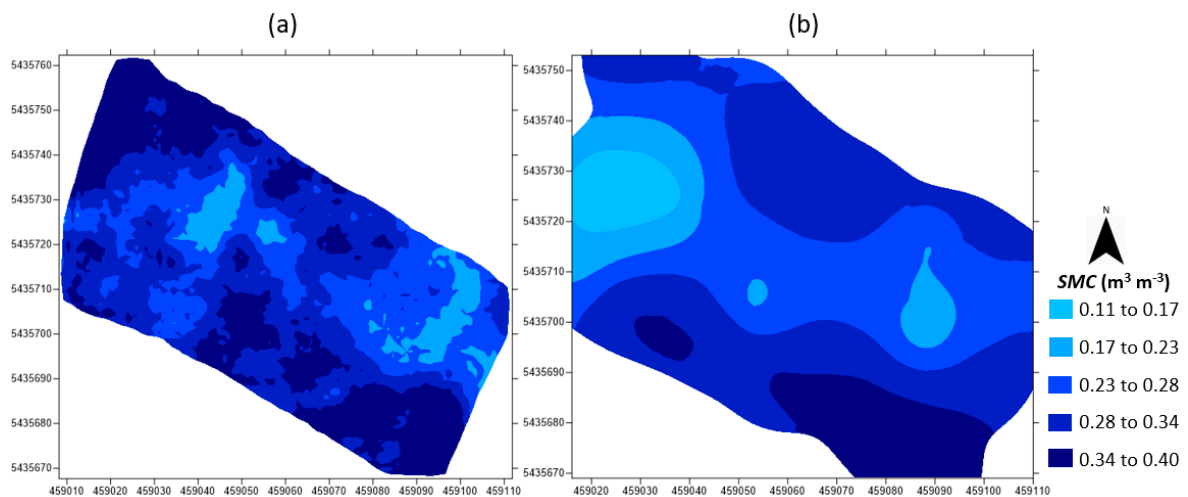


Figure 8. Spatial variability maps of SMC for the large field study estimated using EC_a -L measurements (a) and 27 geo-referenced point measurements using the HD2-TDR (b).

4. Discussion

The factory calibration of HD2-TDR is not sufficient for field applications as it was carried out in a repacked soil with uniform temperature and low bulk electrical conductivity [51]. Also, a low representative elemental volume of soils, which affects the variability of moisture content, has been

reported for many current sensor technologies as well as direct sampling methods [58]. This variability has been attributed to several factors such as gravel content and position in the landscape, which influences water content variation across the field [58]. In this study, visual observations indicated a highly disturbed soil surface and high gravel content at the 0–10 cm soil depth and positions of measurement (point measurements) within the study area. This may be assumed to have led to differences between the 11 cm HD2-TDR probe data and the calculated SMC from the gravimetric SMC (Figure 2). This behaviour implies that it is not a field error (Std Dev = $0.037 \text{ m}^3 \text{ m}^{-3}$), but a high spatial variability of the field water content within the shallow depth.

Khan et al. [43] reported a low EC_a , between 2.1 and 35.5 mS m^{-1} , on an orthic Humo-ferric podzol while Pan et al. [59] indicated a low EC_a between 1.36 and 3.29 mS m^{-1} in a sandy soil. Martini et al. [60] also observed a low EC_a , between 0 and 24 mS m^{-1} , with a very small range of spatial variation which was predominantly attributed to the low heterogeneity of soil texture (Sand = 6%–28%, Silt = 55%–79%, Clay = 13%–25%). These EC_a ranges of previous studies are similar to the results of our study site, classified as an orthic Humo-ferric podzol, with a lower EC_a ranging between 0 and 7 mS m^{-1} and also with a low textural variation (Sand = 80.10%–83.75%, Silt = 10.44%–12.58%, Clay = 5.81%–7.32%). Although the report by Martini et al. [60] has low sand content and variation, the clay content (which is one of the factors that can influence EC_a ; McNeill [20]) is lower at both sites of this study.

The depth range (0–20 cm) considered in this study, also includes the Podzolic Ae horizon with a texture that is coarser than the adjacent horizons [44]. The known depth-response function of CMD-MINIEXPLORER has been used by various authors to calibrate the sensor, even though not all coil separations exhibit low signal to noise levels [33,61].

Arguably, the multi-frequency GEM-2 sensor measures at a deeper DOI compared to the multi-coil CMD-MINIEXPLORER sensor. The measured EC_a from the GEM-2 sensor has lower values compared to the measured EC_a from the CMD-MINIEXPLORER sensor with known DOIs of 90 cm and 180 cm for low (EC_a -L) and high (EC_a -H) coil 3 dipole configurations, respectively. Evaluating the EC_a measurements by GEM-2 with the site soil and parent material using the EMI skin depth, Nomogram [52] also confirmed a greater DOI than 180 cm. When the DOI increases, weaker signals indicate a less conductive soil, whereby stronger signals are observed with decreasing DOI [38,39]. Additionally, the CMD-MINIEXPLORER with the coil 3 dipole configuration adopted in this study shows the highest local sensitivity at a depth between 0–35 cm and 0–75 cm, according to the sensitivity function by McNeil [20]. This provides a reasonable match between the sensing volume of EMI and the depth range sampled by the HD2-TDR precision soil moisture probe, considering the DOI from the soil surface as zero. The largest coil separation in VCP mode was also less sensitive to variations in instrument height that inevitably occurred when EMI measurements were carried out.

Warrick and Nielsen [57] proposed the use of CV categories, which have been widely adopted to assess the soil's spatial variability. This procedure allows for comparisons across samples that employ different units of measurement [62]. However, the geostatistical techniques must be carried out to understand the spatial dependence among the variables [63]. Molin and Faulin [64] found CVs for EC_a and SMC to be moderate (43% and 57%). These findings are similar to the results of this study even though CVs are less than 23% (Table 2). The CVs of EC_a -L, EC_a -H, and EC_a -38 kHz measurements and measured SMC (Table 2) suggest that EC_a values respond to vertical heterogeneity of soil properties [65] such as SMC variability along the soil depth.

Other researchers also found considerable site-to-site variability in the relationship between EC_a and SMC e.g., [25], similar to our study. The R^2 and RMSE of validation models are not consistent when compared to those of calibration models (Table 4). For instance, calibration using $\theta_{v(0-16)}$ produced an R^2 of 0.74 and RMSE of $0.018 \text{ m}^3 \text{ m}^{-3}$ while validation produced R^2 of 0.54 and RMSE of $0.031 \text{ m}^3 \text{ m}^{-3}$. The R^2 generated when the detailed field study regression models were applied to the grass plot showed a need for site-specific calibration to establish the relationship between EC_a and SMC (Table 5). Also, the R^2 and the RMSE values for SMC presented in Figure 6 for EC_a -L, EC_a -H, and

EC_a -38 kHz measurements vary by $0.031 \text{ m}^3 \text{ m}^{-3}$ and $0.040 \text{ m}^3 \text{ m}^{-3}$. This implies that the variation in SMC can be attributed to the maximum sensitivity of the EC_a .

Martini et al. [60] observed that SMC monitoring using EC_a requires the determination of the temporal variations of all other variables that can induce EC_a (e.g., temperature and EC_w) while Altdorff et al. [66] reported that EMI has the potential to account for a strong influence of SMC on EC_a . Even though our study did not account for all variables, the data set used in this study gave a reasonably accurate site-specific calibration of SMC at the study site. However, spatial statistics techniques such as variogram modelling are needed to confirm the number of required sampling points and capture the spatial variability more accurately.

This study confirms the relationship between EC_a and SMC through the correlation between the spatial pattern of EC_a (Figure 7) and SMC (Figure 8). Regions of low EC_a correspond to regions of low SMC and vice versa. For instance, the region with the $EC_a > 5 \text{ mS m}^{-1}$ corresponds to the SMC region $> 0.28 \text{ m}^3 \text{ m}^{-3}$ and the region with $EC_a < 4 \text{ mS m}^{-1}$ corresponds to the SMC region $< 0.23 \text{ m}^3 \text{ m}^{-3}$. The spatial variability of geo-referenced SMC is lower than EC_a -L predicted SMC (Figure 8), as expected. This may indicate the need for more sampling locations to fully capture the spatial variability of SMC and its effects on the map interpolation.

5. Conclusions

Analysis of the relationships between EC_a measurements using two EMI sensors (CMD-MINIEXPLORER and GEM-2), and SMC using oven drying and HD2-TDR methods were carried out on a podzolic soil at an experimental site in western Newfoundland, Canada. Linear regression analysis used to estimate SMC from the two EMI sensors using EC_a data at the study site provided the best prediction for SMC at 0–11 cm and 0–16 cm depth ranges.

The validation results show that to derive reasonably accurate regression models for predicting SMC from EMI measurements for field scale mapping of SMC , sitespecific calibration is required. The site-specific calibration of EC_a - SMC can be determined using linear regression models. This can be attributed to the potential of CMD-MINIEXPLORER and GEM-2 to measure the strong influence of SMC on EC_a implying that the SMC is a major driver of EC_a measurement at the study site.

A good relationship was found between the measured EC_a from CMD-MINIEXPLORER and GEM-2 at the study site. The CMD-MINIEXPLORER and GEM-2 were observed to have similar values for the selected coil orientation and frequency used in this study. Though the temperature effect is minimal, it is important to conduct the direct measurements and EMI measurements from the two EMI sensors within a short period of time as there will be minor changes of SMC .

Further research on the prediction of profile depth and sampling volume at the field needs to be conducted to confirm if SMC is the basic driver of CMD-MINIEXPLORER and GEM-2 response along the depth and horizontal variation at a large scale.

Author Contributions: Conceptualization, L.G.; Data curation, E.B. and L.G.; Formal analysis, E.B.; Funding acquisition, L.G.; Investigation, E.B.; Methodology, E.B. and L.G.; Project administration, L.G.; Resources, M.C., V.K. and L.G.; Supervision, A.U. and L.G.; Writing—original draft, E.B.; Writing—review & editing, A.U., M.C., V.K. and L.G.

Funding: This research was funded by Research and Development Corporation of Newfoundland and Labrador through *Ignite R&D* program 5404-1962-101 and the Research Office of Grenfell Campus, Memorial University of Newfoundland through stat-up fund 20160160.

Acknowledgments: We acknowledge an MSc—BEAS graduate fellowship from Memorial University, E. Badewa, and data-collection support by Marli Vermooten, Dinushika Wanniarachchi and Kamaleswaran Sadatcharam.

Conflicts of Interest: The authors declare no conflict of interest. The funders had no role in the design of the study; in the collection, analyses, or interpretation of data; in the writing of the manuscript, and in the decision to publish the results.

References

1. Corwin, D.L.; Lesch, S.M. Characterizing soil spatial variability with apparent soil electrical conductivity part II. case study. *Comput. Electron. Agric.* **2005**, *46*, 135–152. [[CrossRef](#)]
2. Peralta, N.R.; Costa, J.L. Delineation of management zones with soil apparent electrical conductivity to improve nutrient management. *Comput. Electron. Agric.* **2013**, *99*, 218–226. [[CrossRef](#)]
3. Lesch, S.M.; Corwin, D.L.; Robinson, D.A. Apparent soil electrical conductivity mapping as an agricultural management tool in arid zone soils. *Comput. Electron. Agric.* **2005**, *46*, 351–378. [[CrossRef](#)]
4. Bongiovanni, R.; Lowenberg-DeBoer, J. Precision agriculture and sustainability. *Precis. Agric.* **2004**, *5*, 359–387. [[CrossRef](#)]
5. Kyaw, T.; Ferguson, R.B.; Adamchuk, V.I.; Marx, D.B.; Tarkalson, D.D.; McCallister, D.L. Delineating site-specific management zones for pH-induced iron chlorosis. *Precis. Agric.* **2008**, *9*, 71–84. [[CrossRef](#)]
6. Fortes, R.; Millán, S.; Prieto, M.H.; Campillo, C. A methodology based on apparent electrical conductivity and guided soil samples to improve irrigation zoning. *Precis. Agric.* **2015**, *16*, 441–454. [[CrossRef](#)]
7. Corwin, D.L.; Lesch, S.M. Apparent soil electrical conductivity measurements in agriculture. *Comput. Electron. Agric.* **2005**, *46*, 11–43. [[CrossRef](#)]
8. Doolittle, J.A.; Brevik, E.C. The use of electromagnetic induction techniques in soils studies. *Geoderma* **2014**, *223*, 33–45. [[CrossRef](#)]
9. Galagedara, L.W.; Parkin, G.W.; Redman, J.D.; von Bertoldi, P.; Endres, A.L. Field studies of the GPR ground wave method for estimating soil water content during irrigation and drainage. *J. Hydrol.* **2005**, *301*, 182–197. [[CrossRef](#)]
10. Wijewardana, Y.G.N.S.; Galagedara, L.W. Estimation of spatio-temporal variability of soil water content in agricultural fields with ground penetrating radar. *J. Hydrol.* **2010**, *391*, 24–33. [[CrossRef](#)]
11. Topp, G.C.; Davis, J.L.; Annan, A.P. Electromagnetic determination of soil water content: Measurements in coaxial transmission lines. *Water Resour. Res.* **1980**, *16*, 574–582. [[CrossRef](#)]
12. Ferré, P.A.; Redman, J.D.; Rudolph, D.L.; Kachanoski, R.G. The dependence of the electrical conductivity measured by time domain reflectometry on the water content of a sand. *Water Resour. Res.* **1998**, *34*, 1207–1213. [[CrossRef](#)]
13. Desilets, D.; Zreda, M.; Ferre, T.P.A. Nature's neutron probe: Land surface hydrology at an elusive scale with cosmic rays. *Water Resour. Res.* **2010**. [[CrossRef](#)]
14. Franz, T.E.; Zreda, M.; Ferre, P.A.; Rosolem, R. An assessment of the effect of horizontal soil moisture heterogeneity on the area-average measurement of cosmic-ray neutrons. *Water Resour. Res.* **2013**, *49*, 1–10. [[CrossRef](#)]
15. Mondal, P.; Tewari, V.K. Present status of precision farming: A review. *Int. J. Agric. Res.* **2007**, *5*, 1124–1133.
16. Jay, S.C.; Lawrence, R.L.; Repasky, K.S.; Rew, L.J. Detection of leafy spurge using hyper-spectral-spatial-temporal imagery. In Proceedings of the 2010 IEEE International Geoscience and Remote Sensing Symposium, Honolulu, HI, USA, 25–30 July 2010; IEEE: Bozeman, MT, USA; pp. 4374–4376.
17. Zhang, Z.; He, G.; Jiang, H. Leaf area index retrieval using red edge parameters based on Hyperion hyper-spectral imagery. *J. Theor. Appl. Inf. Technol.* **2013**, *48*, 957–960.
18. Rudolph, S.; van der Kruk, J.; von Hebel, C.; Ali, M.; Herbst, M.; Montzka, C.; Pätzold, S.; Robinson, D.A.; Vereecken, H.; Weihermüller, L. Linking satellite derived LAI patterns with subsoil heterogeneity using large-scale ground-based electromagnetic induction measurements. *Geoderma* **2015**, *241–242*, 262–271. [[CrossRef](#)]
19. Rhoades, J.D.; Raats, P.A.; Prather, R.J. Effects of liquid-phase electrical conductivity, water content, and surface conductivity on bulk soil electrical conductivity. *Soil Sci. Soc. Am. J.* **1976**, *40*, 651–655. [[CrossRef](#)]
20. McNeill, J.D. *Electromagnetic Terrain Conductivity Measurement at Low Induction Numbers*; Geonics Ltd.: Mississauga, ON, Canada, 1980.
21. Kachanoski, R.G.; Gregorich, E.G.; van Wesenbeeck, I.J. Estimating spatial variations of soil water content using non contacting electromagnetic inductive methods. *Can. J. Soil Sci.* **1988**, *68*, 715–722. [[CrossRef](#)]
22. Brevik, E.C.; Fenton, T.E. The relative influence of soil water, clay, temperature, and carbonate minerals on soil electrical conductivity readings with an EM-38 along a Mollisol catena in central Iowa. *Soil Surv. Horiz.* **2002**, *43*, 9–13. [[CrossRef](#)]

23. Corwin, D.L.; Lesch, S.M. Application of soil electrical conductivity to precision agriculture. *Agron. J.* **2003**, *95*, 455–471. [[CrossRef](#)]
24. Friedman, S.P. Soil properties influencing apparent electrical conductivity: A review. *Comput. Electron. Agric.* **2005**, *46*, 45–70. [[CrossRef](#)]
25. Brevik, E.C.; Fenton, T.E.; Lazari, A. Soil electrical conductivity as a function of soil water content and implications for soil mapping. *Precis. Agric.* **2006**, *7*, 393–404. [[CrossRef](#)]
26. Serrano, J.M.; Shahidian, S.; da Silva, J.R.M. Apparent electrical conductivity in dry versus wet soil conditions in a shallow soil. *Precis. Agric.* **2013**, *14*, 99–114. [[CrossRef](#)]
27. Huang, J.; Scudiero, E.; Bagtang, M.; Corwin, D.L.; Triantafilis, J. Monitoring scale-specific and temporal variation in electromagnetic conductivity images. *Irrig. Sci.* **2016**, *34*, 187–200. [[CrossRef](#)]
28. Altdorff, D.; Galagedara, L.; Nadeem, M.; Cheema, M.; Unc, A. Effect of agronomic treatments on the accuracy of soil moisture mapping by electromagnetic induction. *Catena* **2018**, *164*, 96–106. [[CrossRef](#)]
29. Lesch, S.M.; Strauss, D.J.; Rhoades, J.D. Spatial prediction of soil salinity using electromagnetic induction techniques. Part 1. Statistical prediction models: A comparison of multiple linear regression and cokriging. *Water Resour. Res.* **1995**, *31*, 373–386. [[CrossRef](#)]
30. Goff, A.; Huang, J.; Wong, V.N.L.; Monteiro Santos, F.A.; Wege, R.; Triantafilis, J. Electromagnetic conductivity imaging of soil salinity in an estuarine–Alluvial landscape. *Soil Sci. Soc. Am. J.* **2014**, *78*, 1686. [[CrossRef](#)]
31. Lesch, S.M.; Corwin, D.L. Predicting EM/soil property correlation estimates via the dual pathway parallel conductance model. *Agron. J.* **2003**, *95*, 365–379. [[CrossRef](#)]
32. Walter, J.; Lueck, E.; Bauriegel, A.; Richter, C.; Zeitz, J. Multi-scale analysis of electrical conductivity of peatlands for the assessment of peat properties. *Eur. J. Soil Sci.* **2015**, *66*, 639–650. [[CrossRef](#)]
33. Altdorff, D.; Bechtold, M.; van der Kruk, J.; Vereecken, H.; Huisman, J.A. Mapping peat layer properties with multi-coil offset electromagnetic induction and laser scanning elevation data. *Geoderma* **2016**, *261*, 178–189. [[CrossRef](#)]
34. Bittelli, M. Measuring soil water content: A review. *HortTechnology* **2011**, *21*, 293–300.
35. Huang, J.; Nhan, T.; Wong, V.N.L.; Johnston, S.G.; Lark, R.M.; Triantafilis, J. Digital soil mapping of a coastal acid sulfate soil landscape. *Soil Res.* **2014**, *52*, 327–339. [[CrossRef](#)]
36. Vereecken, H.; Huisman, J.A.; Pachepsky, Y.; Montzka, C.; Van Der Kruk, J.; Bogaen, H.; Weihermüller, L.; Herbst, M.; Martinez, G.; Vanderborght, J. On the spatio-temporal dynamics of soil moisture at the field scale. *J. Hydrol.* **2014**, *516*, 76–96. [[CrossRef](#)]
37. Allred, B.J.; Ehsani, M.R.; Saraswat, D. The impact of temperature and shallow hydrologic conditions on the magnitude and spatial pattern consistency of electromagnetic induction measured soil electrical conductivity. *Am. Soc. Agric. Eng.* **2005**, *48*, 2123–2135. [[CrossRef](#)]
38. Callegary, J.B.; Ferré, T.P.A.; Groom, R.W. Vertical spatial sensitivity and exploration depth of low-induction-number electromagnetic induction instruments. *Vadose Zone J.* **2007**, *6*, 158–167. [[CrossRef](#)]
39. Delefortrie, S.; Saey, T.; Van De Vijver, E.; De Smedt, P.; Missiaen, T.; Demerre, I.; Van Meirvenne, M. Frequency domain electromagnetic induction survey in the intertidal zone: Limitations of low-induction-number and depth of exploration. *J. Appl. Geophys.* **2014**, *100*, 14–22. [[CrossRef](#)]
40. Horney, R.D.; Taylor, B.; Munk, D.S.; Roberts, B.A.; Lesch, S.M.; Plant, R.E. Development of practical site-specific management methods for reclaiming salt-affected soil. *Comput. Electron. Agric.* **2005**, *46*, 379–397. [[CrossRef](#)]
41. Triantafilis, J.; Terhune IV, C.H.; Monteiro Santos, F.A. An inversion approach to generate electromagnetic conductivity images from signal data. *Environ. Model. Softw.* **2013**, *43*, 88–95. [[CrossRef](#)]
42. Singh, G.; Williard, K.W.; Schoonover, J.E. Spatial relation of apparent soil electrical conductivity with crop yields and soil properties at different topographic positions in a small agricultural watershed. *Agronomy* **2016**, *6*, 57. [[CrossRef](#)]
43. Khan, F.S.; Zaman, Q.U.; Chang, Y.K.; Farooque, A.A.; Schumann, A.W.; Madani, A. Estimation of the rootzone depth above a gravel layer (in wild blueberry fields) using electromagnetic induction method. *Precis. Agric.* **2016**, *17*, 155–167. [[CrossRef](#)]
44. Soil Classification Working Group. *The Canadian System of Soil Classification*, 3rd ed.; Agriculture and Agri-Food Canada Publication: Ottawa, ON, Canada, 1998.
45. Driessen, P.; Deckers, J.; Spaargaren, O.; Nachtergaele, F. *Lecture Notes on the Major Soils of the World*; Food and Agriculture Organization of the United Nations (FAO): Rome, Italy, 2001.

46. Sanborn, P.; Lamontagne, L.; Hendershot, W. Podzolic soils of Canada: Genesis, distribution, and classification. *Can. J. Soil Sci.* **2011**, *91*, 843–880. [[CrossRef](#)]
47. King, M.; Altdorff, D.; Li, P.; Galagedara, L.; Holden, J.; Unc, A. Northward shift of the agricultural climate zone under 21st-century global climate change. *Sci. Rep.* **2018**. [[CrossRef](#)] [[PubMed](#)]
48. Wang, C.; Rees, H.W.; Daigle, J.L. Classification of podzolic soils as affected by cultivation. *Can. J. Soil Sci.* **1984**, *64*, 229–239. [[CrossRef](#)]
49. Altdorff, D.; Galagedara, L.; Unc, A. Impact of projected land conversion on water balance of boreal soils in western Newfoundland. *J. Water Clim. Chang.* **2017**. [[CrossRef](#)]
50. Kirby, G.E. In *Soils of the Pasadena-Deer Lake Area, Newfoundland*. 1988. Available online: http://sis.agr.gc.ca/cansis/publications/surveys/nf/nf17/nf17_report.pdf (accessed on 7 November 2016).
51. IMKO. TRIME-TDR User Manual. Available online: <https://imko.de/en/about-trime-tdr> (accessed on 8 December 2016).
52. Won, I.J. A wide-band electromagnetic exploration method—Some theoretical and experimental results. *Geophysics* **1980**, *45*, 928–940. [[CrossRef](#)]
53. Ma, R.; McBratney, A.; Whelan, B.; Minasny, B.; Short, M. Comparing temperature correction models for soil electrical conductivity measurement. *Precis. Agric.* **2011**, *12*, F55–F66. [[CrossRef](#)]
54. Robinson, D.A.; Lebron, I.; Lesch, S.M.; Shouse, P. Minimizing drift in electrical conductivity measurements in high temperature environments using the EM-38. *Soil Sci. Soc. Am. J.* **2004**, *68*, 339–345. [[CrossRef](#)]
55. GF Instruments. CMD Electromagnetic Conductivity Meter User Manual V. 1.5. Geophysical Equipment and Services, Czech Republic, 2011. Available online: http://www.gfinstruments.cz/index.php?menu=gi&smenu=iem&cont=cmd_&ear=ov (accessed on 4 June 2016).
56. Zhu, Q.; Lin, H.; Doolittle, J. Repeated electromagnetic induction surveys for determining subsurface hydrologic dynamics in an agricultural landscape. *Soil Sci. Soc. Am. J.* **2010**, *74*, 1750–1762. [[CrossRef](#)]
57. Warrick, A.W.; Nielsen, D.R. Spatial variability of soil physical properties in the field. In *Applications of Soil Physics*; Hillel, D., Ed.; Academic Press: New York, NY, USA, 1980; pp. 319–344.
58. Hignett, C.; Evett, S. Direct and Surrogate Measures of Soil Water Content. International Atomic Energy Agency, Soil and Water Management and Crop Nutrition Section, Vienna (Austria). No. IAEA-TCS-30. 2008. Available online: http://www-pub.iaea.org/MTCD/publications/PDF/TCS-30_web.pdf (accessed on 8 September 2016).
59. Pan, L.; Adamchuk, V.I.; Prasher, S.; Gebbers, R.; Taylor, R.S.; Dabas, M. Vertical soil profiling using a galvanic contact resistivity scanning approach. *Sensors* **2014**, *14*, 13243–13255. [[CrossRef](#)] [[PubMed](#)]
60. Martini, E.; Werban, U.; Zacharias, S.; Pohle, M.; Dietrich, P.; Wollschläger, U. Repeated electromagnetic induction measurements for mapping soil moisture at the field scale: Validation with data from a wireless soil moisture monitoring network. *Hydrol. Earth Syst. Sci.* **2017**, *21*, 495. [[CrossRef](#)]
61. Bonsall, J.; Fry, R.; Gaffney, C.; Armit, I.; Beck, A.; Gaffney, V. Assessment of the CMD mini-explorer, a new low-frequency multi-coil electromagnetic device, for archaeological investigations. *Archaeol. Prospect.* **2013**, *20*, 219–231. [[CrossRef](#)]
62. Souza, Z.M.D.; Marques Júnior, J.; Pereira, G.T. Spatial variability of the physical and mineralogical properties of the soil from the areas with variation in landscape shapes. *Braz. Arch. Biol. Technol.* **2009**, *52*, 305–316. [[CrossRef](#)]
63. Liu, T.L.; Juang, K.W.; Lee, D.Y. Interpolating soil properties using kriging combined with categorical information of soil maps. *Soil Sci. Soc. Am. J.* **2006**, *70*, 1200–1209. [[CrossRef](#)]
64. Molin, J.P.; Faulin, G.D.C. Spatial and temporal variability of soil electrical conductivity related to soil moisture. *Sci. Agricola* **2013**, *70*, 1–5. [[CrossRef](#)]
65. Neely, H.L.; Morgan, C.L.; Hallmark, C.T.; McInnes, K.J.; Molling, C.C. Apparent electrical conductivity response to spatially variable vertisol properties. *Geoderma* **2016**, *263*, 168–175. [[CrossRef](#)]
66. Altdorff, D.; von Hebel, C.; Borchard, N.; van der Kruk, J.; Bogena, H.R.; Vereecken, H.; Huisman, J.A. Potential of catchment-wide soil water content prediction using electromagnetic induction in a forest ecosystem. *Environ. Earth Sci.* **2017**, *76*, 111. [[CrossRef](#)]

